

# Computational Analysis of the Effects of Exercise on Hemodynamics in the Carotid Bifurcation

H. F. YOUNIS,<sup>1</sup> M. R. KAAZEMPUR-MOFRAD,<sup>1</sup> C. CHUNG,<sup>1</sup> R. C. CHAN,<sup>2</sup> and R. D. KAMM<sup>1</sup>

<sup>1</sup>Department of Mechanical Engineering and the Division of Biological Engineering, Massachusetts Institute of Technology, Cambridge, MA and <sup>2</sup>Boston Heart Foundation, Harvard/MIT Division of Health Sciences and Technology, Cambridge, MA

(Received 3 April 2002; accepted 16 April 2003)

**Abstract**—The important influence of hemodynamic factors in the initiation and progression of arterial disease has led to numerous studies to computationally simulate blood flow at sites of disease and examine potential correlative factors. This study considers the differences in hemodynamics produced by varying heart rate in a fully coupled fluid-structure three-dimensional finite element model of a carotid bifurcation. Two cases with a 50% increase in heart rate are considered: one in which peripheral resistance is uniformly reduced to maintain constant mean arterial pressure, resulting in an increase in mean flow, and a second in which cerebral vascular resistance is held constant so that mean carotid artery flow is nearly unchanged. Results show that, with increased flow rate, the flow patterns are relatively unchanged, but the magnitudes of mean and instantaneous wall shear stress are increased roughly in proportion to the flow rate, except at the time of minimum flow (and maximum flow separation) when shear stress in the carotid bulb is increased in magnitude more than threefold. When cerebral peripheral resistance is held constant, the differences are much smaller, except again at end diastole. Maximum wall shear stress temporal gradient is elevated in both cases with elevated heart rate. Changes in oscillatory shear index are minimal. These findings suggest that changes in the local hemodynamics due to mild exercise may be relatively small in the carotid artery. © 2003 Biomedical Engineering Society. [DOI: 10.1114/1.1590661]

**Keywords**—Exercise, Atherosclerosis, Finite element analysis, Carotid bifurcation, Blood flow, Wall shear stress.

## INTRODUCTION

Due to the strong correlations known to exist between sites of atherosclerosis and variations in local hemodynamics, considerable research has been performed to date on arterial blood flow in bifurcations, junctions, and grafts. These studies include numerical simulations that allow detailed and direct examination of the flow and shear stress patterns in regions of interest. In a continuing attempt to increase the realism of these simulations, new factors have been introduced including non-

Newtonian blood properties, arterial wall compliance, and at times, treating the blood as a two-phase medium. Each added factor represents another step toward a realistic prediction of wall shear stress (and other related parameters), so that these might be correlated with measures of disease or the various biological factors known to cause it.

For example, a study by Gijsen *et al.*<sup>14</sup> on the influence of non-Newtonian properties of steady blood flow in the carotid bifurcation demonstrated that notable differences exist between Newtonian and non-Newtonian models. The axial velocity field of the non-Newtonian fluid was flattened, and it had higher velocity gradients at the outside wall and lower gradients at the flow divider than the Newtonian model. On the other hand, Perktold *et al.*<sup>28</sup> found that in the case of pulsatile flow, the general flow characteristics between Newtonian and non-Newtonian models were largely unchanged in the carotid bifurcation. An experimental investigation by Friedman *et al.*<sup>11</sup> supported this conclusion by noting that the effect of fluid rheology in the aortic bifurcation is minimal in quantifying the correlation between intimal thickening and shear rate.

Another aspect of arterial blood flow that has been much investigated is the effect of arterial wall compliance on the flow characteristics. Friedman *et al.*<sup>11</sup> demonstrated that the effect of compliance is also insignificant. Steinman and Ethier<sup>30</sup> have observed that only minor changes in overall wall shear stress patterns occurred when the effect of wall distensibility was included in an end-to-side anastomosis. In separate simulations, Perktold and colleagues<sup>27</sup> demonstrated that flow separation and wall shear stress are reduced in a distensible wall model of the carotid bifurcation. Consistent with Perktold *et al.*<sup>27</sup> and Zhao *et al.*,<sup>35</sup> wall distensibility was found to have little effect on the wall shear stress patterns at the outer wall of the carotid bulb, generally believed to be the site most prone to disease. Significant differences in wall shear stress, of up to 25%, only appeared at the flow divider.<sup>27</sup>

Address correspondence to Roger D. Kamm, 77 Massachusetts Avenue, Room 3-260, Cambridge, MA 02139. Electronic mail: rdkamm@mit.edu

Despite the large number of previous studies, only a few have rigorously examined the effect of normal, daily variations in local hemodynamic conditions.<sup>19,23–25</sup> This is rather surprising since one might expect these variations, due to large changes in cardiac output, to far exceed the small effects associated with non-Newtonian rheology or even wall compliance. Depending on the level of activity and the variations that an individual experiences during the course of a day, changes in mean blood flow rate might expectedly cause more significant variations in the above-mentioned parameters. In addition, due to the effect of pulse wave reflections on shaping the local pressure waveform, even the pattern of pressure and velocity variations will change. These variations are not only due to intense exercise, but can even be seen in mild exertion such as brisk walk. Here, we consider these effects in the context of blood flow through a healthy carotid bifurcation.

## METHODS

Pulsatile blood flow in a model carotid bifurcation is simulated using fully coupled fluid–structure interaction finite element methods at two different heart rates: 72 bpm representing a person at rest and the other at 108 bpm (50% increase). Two cases are considered at 108 bpm heart rate: (a) peripheral resistance is uniformly reduced resulting in an increase in mean flow, and (b) peripheral resistance reduced, except in the brain where it is held constant and, hence, mean flow to carotid artery is nearly unchanged. For each case, wall shear stress values, relevant integrated parameters of wall shear stress over the cycle as well as temporal gradients of wall shear stress are compared to identify significant differences among them.

### Material Models and Solution Process

The simulations employ finite element analysis (ADINA, version 7.3, Automatic Dynamic Incremental Nonlinear Analysis, Watertown, MA) and incorporate a nonlinear, isotropic, hyperelastic model for the arterial wall. Blood is treated as an incompressible, Newtonian fluid (an assumption that has repeatedly been shown to hold well for large arteries,<sup>4,28</sup> where shear rates generally exceed  $100 \text{ s}^{-1}$ ) and the flow is assumed laminar.

The arterial solid response is modeled using the standard Lagrangian formulation for large displacements and large strains.<sup>2</sup> An isotropic form of the strain energy density function for the (nearly) incompressible artery wall is specified.<sup>9</sup>

$$W = \frac{a}{b} [e^{[b/2(I_1 - 3)]} - 1], \quad (1)$$

where  $a$  and  $b$  ( $a = 44.25 \text{ kPa}$ ,  $b = 16.73$ ) are elastic constants that reflect the elastic properties and tissue composition; their values are obtained using a nonlinear regression fit to pressure–diameter inflation tests of the carotid artery.<sup>8,31</sup>  $I_1$  is the first invariant of the strain tensor. In the Taylor series expansion,  $a$  has the significance of the elastic modulus. This exponential form is appropriate for arterial mechanics since it portrays the well-known strain-stiffening behavior of collagen.

Continuity and the full Navier–Stokes equations are solved for the fluid. For fluid domains with moving boundaries, we utilize the arbitrary Lagrangian Eulerian (ALE) formulation of the momentum equation.<sup>2</sup> Full coupling between the fluid and solid domains requires that displacement continuity and force equilibrium are satisfied at the fluid–structure interface at each step. This is done iteratively between the fluid and structure solvers at each time step until sufficient convergence is reached.

Fluid–structure interaction analysis is generally important when large scale motions of the arteries are present and impact the flow field considerably, as in studies of arterial collapse when largely obstructive stenoses are present<sup>3,10</sup> or where physiologic movement of blood vessels (e.g., coronary arteries) during the cardiac cycle affects blood flow patterns significantly.<sup>22</sup> In the carotid bifurcation, even though the motions due to arterial wall motion are relatively small, wall compliance can have a locally significant effect (up to 25% difference in wall shear stress) at the divider wall<sup>27</sup> and was thus included in the simulations herein. The results presented focus on the fluid domain; the arterial wall strain distributions are presented elsewhere.<sup>34</sup>

### Model Description and Boundary Conditions

An idealized but realistic three-dimensional (3D) solid model of the carotid bifurcation (extending from 3 cm distal to 3 cm proximal to the bifurcation) based on the work of Bharadvaj *et al.*<sup>6,7</sup> and Delfino *et al.*<sup>9</sup> was created in SolidWorks (SolidWorks Corporation, Concord, MA) and imported into the finite element software for meshing and analysis. Only half of the geometry was modeled and symmetry boundary conditions were employed. The (solid) model used and boundary conditions imposed are illustrated in Fig. 1. The arterial wall was meshed with an unstructured grid consisting of 43,334 eleven-noded 3D tetrahedral elements and 118,229 nodes. The fluid domain was filled with an unstructured grid consisting of 56,209 four-noded tetrahedral elements with 11,597 nodes. The meshes used for the fluid and solid domains are shown in Fig. 2. Computations were performed using a SGI Origin 2000 computer equipped with 4 processors and 6 GB of RAM.

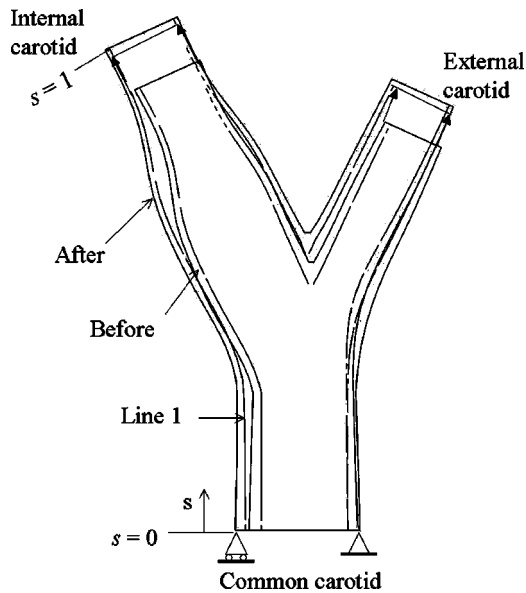


**FIGURE 1.** Idealized model of the carotid bifurcation used for fluid–structure interaction (FSI) simulations showing boundary conditions imposed on the arterial wall (see the text for description of fluid boundary conditions). Due to symmetry, a half model of the carotid bifurcation was utilized. “P” represents the inner surfaces, where the FSI boundary condition was applied. The solid arrows represent an applied axial strain of 10%. Comparisons in wall shear stress are conducted along “line 1” labeled above which spans the entire length (along the normalized coordinate variable  $s$ ) of the common-internal wall, including the carotid bulb.

The fluid–structure simulations were performed in two stages: An “inflation” stage (from 0 to 1 s) in which the fluid velocity vectors were ramped up from zero to diastolic values and within which simultaneously an axial stretch of 10% (as measured *in situ* by Delfino<sup>8</sup>) was applied incrementally to the solid domain (and subsequently stretched the fluid domain). This was followed by the “transient” stage, in which the results from the “inflation” stage were used as initial conditions; the arterial wall stretch remained fixed at 10% and the fluid velocity pulsatile boundary conditions were applied. To achieve a periodic solution, the transient stage flow computation was allowed to run over two heart cycles, saving only the second one. The boundary conditions (flow rate and blood pressure profiles—see Fig. 3) to the transient stage were obtained using the one-dimensional (1D) arterial model of Ozawa *et al.*<sup>26</sup> This is a 32 segment, linked piecewise 1D model of the entire arterial network which has been shown to reproduce the flow and pressure waveforms observed at various locations in the body.<sup>35</sup> Using this model, two situations were simulated, thought to bracket the behavior in the carotid bifurcation. In the first, the heart rate was increased while reducing systemic vascular resistance to keep the mean arterial pressure nearly constant (13 kPa in the 72 bpm vs. 12 kPa in the 108 bpm case), thus causing cardiac output to

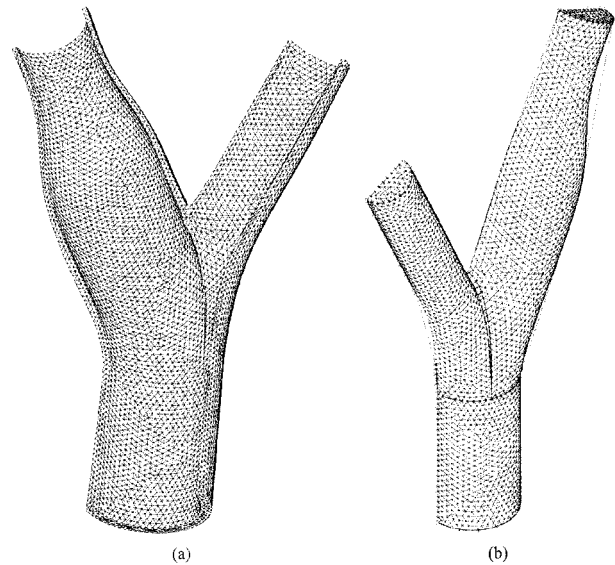


**FIGURE 2.** Finite element meshes used for the solid (a) and fluid (b) domains.

increase. Mean flow rate in the common carotid artery increased by 31% from 12.5 ml/s (72 bpm) to 16.4 ml/s (108 bpm). A second, somewhat more realistic representation of exercise is achieved by following this same procedure, but holding peripheral vascular resistance to the brain fixed on the assumption that during exercise, the largest changes in peripheral resistance are confined to the exercising muscle. Consequently, the primary effects influencing flow conditions are the increase in heart rate and the change in flow and pressure waveform while the mean flow is maintained constant.

The transient stage was subsequently solved in two more steps, similar to the commonly used procedure first introduced by Perktold *et al.*<sup>28</sup> To achieve arterial pulsatility, the pressure profiles shown in Fig. 3 were superimposed on the overall pressure drops across the domain as computed in the inflation/stretch procedure. Following Perktold *et al.*,<sup>28</sup> a Womersley-type flow corresponding to the flow rate profile in the common carotid artery<sup>15</sup> was first imposed node by node at the inlet to the common carotid and a plug flow was specified at the exit of the internal carotid, while the external carotid was specified as having zero normal traction. Flow profiles at the output of the external carotid artery at the end of this step were then used as a boundary condition to the second computational step of this “transient” stage, while retaining Womersley flow at the common carotid and imposing a traction-free boundary condition at the internal carotid. This second step was then considered the final computed solution.<sup>28</sup> The entire procedure was repeated three times; first for 72 bpm and then for the two cases at 108 bpm.

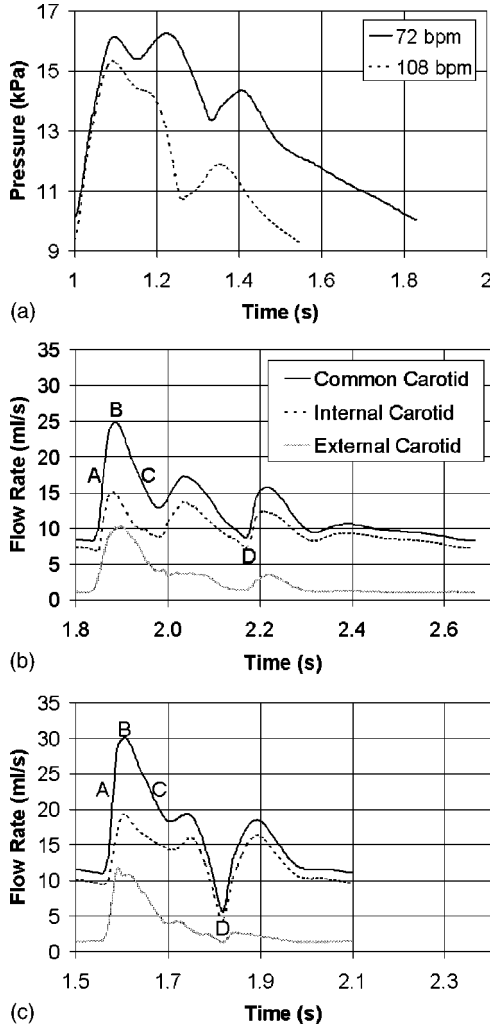


**FIGURE 3.** Pressure (top panel) and flow rate boundary conditions on the fluid domain representing two states: 72 bpm (middle panel) and 108 bpm (lower panel) as obtained from the 1D distributed arterial tree model of Ozawa *et al.* (Ref. 26). Labeled points for comparison are: accelerative (a), peak flow (b) and decelerative (c) phase of systole as well as the point of lowest flow rate (d).

Wall shear stress, oscillatory shear index and maximum wall shear stress temporal gradients are then computed for comparison between the two cases. “Size” of the recirculation region is defined as the normalized length along the common-internal carotid adjoining wall (line 1 of Fig. 1), which exhibits reversed shear stress. It is normalized to the entire length of the common-internal carotid adjoining wall as simulated in the model, with the carotid bulb spanning the nondimensional length  $s = 0.40\text{--}0.73$ , where  $s$  is measured along line 1. The parameter  $s$  denotes the normalized length along the line 1, with  $s=0$  at the inlet to the common carotid artery.

The wall shear stress components are calculated as (using the Einstein summation convention):

$$\tau_i = T_i - (T_j n_j) n_i, \quad (2)$$

where  $T_j = 2\mu e_{jj} n_i$  is the net traction vector at a point on the wall with the local surface normal  $\vec{n}$  and the symmetric rate of strain tensor  $e_{ij}$ . Both the instantaneous,  $\tau_w$  and the temporal mean  $(\tau_w)_{\text{ave}}$  values of wall shear stress are used in the results.

Maximum  $\tau_w$  temporal gradient  $(\partial\tau_w/\partial t)_{\text{max}}$  is the maximum value of the gradient in wall shear stress calculated between every two consecutive time points during the cycle:  $(\partial\tau_w/\partial t)_{\text{max}}$  is defined as

$$\max \left| \frac{\partial \|\tau_w\|}{\partial t} \right|,$$

where  $\|\tau_w\|$  is the magnitude of the local shear stress vector.

The oscillatory shear index (OSI) is a nondimensional measure that quantifies the fractional time a particular wall region in the cycle experiences cross or reverse flow. The mean flow direction is defined by the temporal mean of the shear stress vector. For purely oscillatory flow, the OSI approaches 0.5.<sup>17,25</sup> OSI is defined as

$$\text{OSI} = \frac{\int_0^T \|\tau_w^*\| dt}{\int_0^T \|\tau_w\| dt}, \quad (3)$$

where  $\tau_w^*$  is the component of wall shear stress acting in a direction opposite to the temporal mean value. Note that the OSI does not take into account the magnitude of the shear stress vectors, only the directions.

## RESULTS

### Wall Shear Stress

Previous studies suggest that the hemodynamic parameter of greatest relevance to atherogenesis is the magnitude of the wall shear stress vector.<sup>18</sup> This is presented in the form of band plots of the wall shear stress averaged over the cycle  $(\tau_w)_{\text{ave}}$  for the 72 bpm (case 1) and 108 bpm (cases 2 and 3 for the high and low flow rates, respectively) solutions (Fig. 4). Comparing first cases 1 and 2,  $(\tau_w)_{\text{ave}}$  increases due to the higher flow rate, ranging up to 50% but generally in the range of 20%–30% at the higher heart rate depending on location. Also of note is that the area of low  $(\tau_w)_{\text{ave}} (< 1.0 \text{ Pa})$  shrinks considerably with increasing heart rate (108 bpm vs. 72 bpm). Overall, shear stress levels in the common carotid are uniform and the increase in  $(\tau_w)_{\text{ave}}$  in the 108 bpm case 2 over the 72 bpm case 1 ( $\sim 2.3 \text{ Pa}$  vs.  $1.8 \text{ Pa}$ , respectively) almost directly reflects the 30% increase in average flow rate. When cranial resistance is held constant, however, these differences largely disappear. The

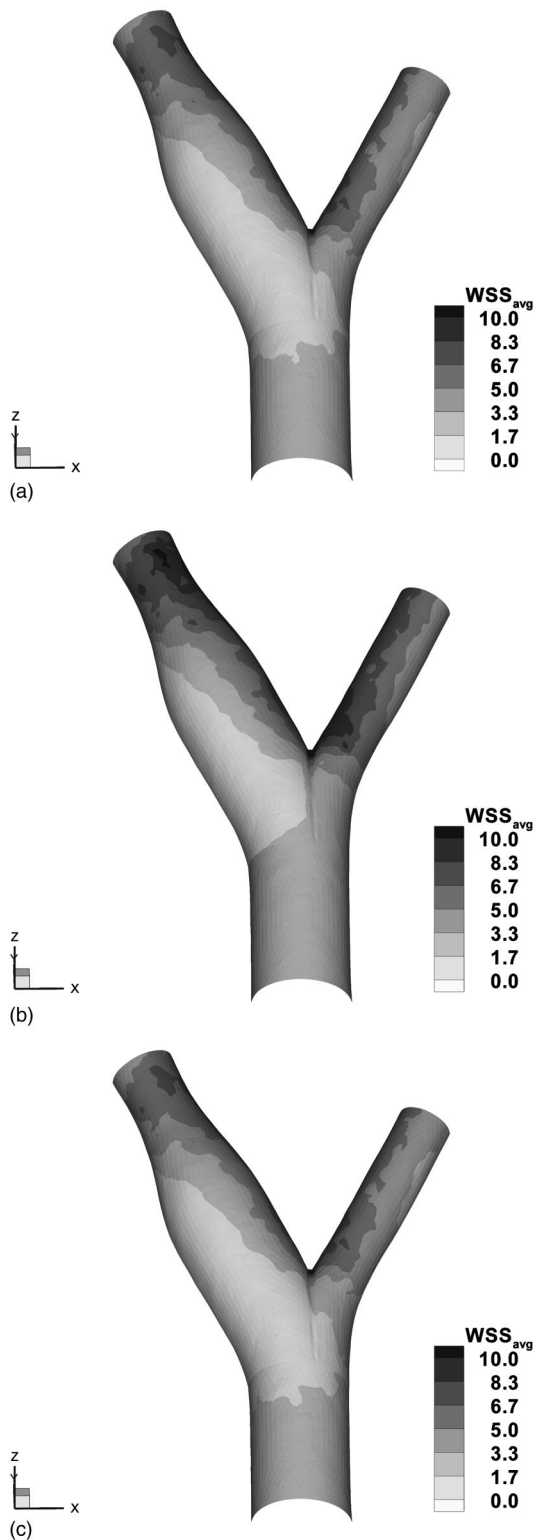
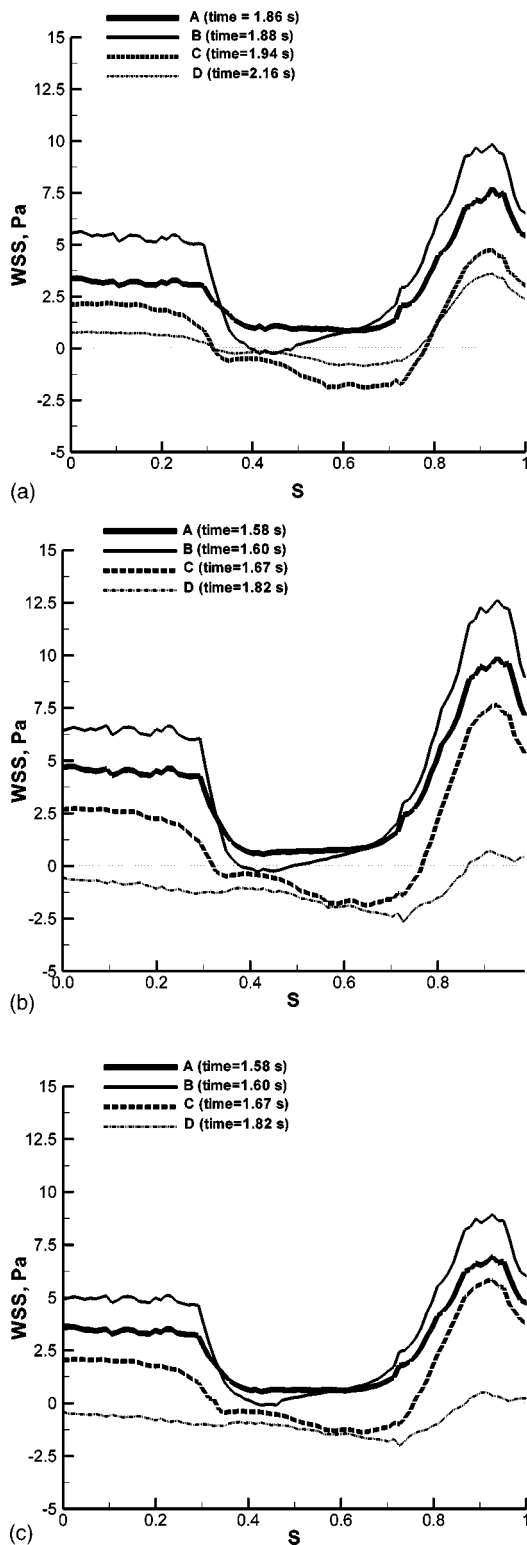


FIGURE 4. Wall shear stress ( $WSS = \tau_w$ ) plots averaged over the entire cardiac cycle: 72 bpm (a); 108 bpm [(b) and (c)].

band plots of  $(\tau_w)_{ave}$  for these two cases are virtually indistinguishable [Figs. 4(a) and 4(c)], despite the higher frequency, and the corresponding increase in Womersley number.

It is of particular interest to consider the outer wall of the carotid bifurcation from the common trunk to the internal carotid (line 1 on Fig. 1), which spans the carotid bulb, a commonly diseased site. The time points chosen for comparison are at peak acceleration (A), peak flow (B), and peak deceleration (C), as well as the time of lowest flow rate (D), which occurs at the flow rate through following the second peak [Fig. 3(b)]. Instantaneous values of  $\tau_w$  along line 1 at these several time points exhibit a general similarity despite the considerable difference in frequency and, for case 2, flow rate (Fig. 5). Flow separation is observed in the carotid bulb starting approximately at time (B) and continuing until a time during flow acceleration prior to time (A). Point (D) is the time at which there exists the largest recirculation zone for all three cases, although at the higher frequency, the region of reverse flow extends all the way to the entrance of the model. Values of  $\tau_w$  in the common carotid generally reflect the relative flow rates, with cases 1 and 3 being most similar and case 2 somewhat greater in magnitude. Values in the carotid bulb tend also to be similar, except that the time of maximum negative shear stress shifts from time (C) to time (D) at the higher frequency, cases 2 and 3. Times (A) and (C) were chosen so that they correspond to approximately the same flow rate, but shear stress is markedly lower at all locations and for all three cases during flow deceleration. Table 1 summarizes the wall shear stress values and normalized lengths of the recirculation regions along this line.

The highest values of  $\tau_w$  in the carotid bulb occur during peak flow, but only at the ends of the bulb region as separation has already started near the upstream end. In the 72 bpm case, the maximum  $\tau_w$  in the bulb over the cycle occurs at the time of peak systolic flow rate (B) and is 2.9 Pa. This compares favorably with the 108 bpm case, where it also occurs at time (B) and has a value of 3.0 Pa. Comparing the values at similar points in the cycle between the two heart rates, we also see some difference in  $\tau_w$  during the accelerative phase of systole (A) (2.0, 2.5 and 1.8 Pa for cases 1, 2, and 3, respectively) that scale approximately with flow rate. However, both at peak systole (B) and during the decelerative phase of systole (C), virtually no difference is observed in  $\tau_w$  as heart rate is increased along with flow rate (case 2), and roughly a 20% decrease is observed as the heart rate is increased while flow rate is maintained constant (case 3). The most significant difference is experienced at the point of lowest flow rate (D) where  $\tau_w$  increases by 225% to 2.6 Pa in case 2 or by 137% to 1.8 Pa in case 3.



**FIGURE 5.** Wall shear stress ( $WSS = \tau_w$ ) along the wall of the common-internal carotid (along line 1 of Fig. 1) at different time points (A,B,C, and D as identified in Fig. 3): 72 bpm (a); 108 bpm [(b) and (c)].

Even though the overall size of the recirculation region over the entire cycle is relatively unaffected by heart rate (see the OSI plots in Fig. 6), there are some variations during the cardiac cycle. In general, increasing the heart rate has mixed effects on the length of the recirculation zone (see Table 1). At the time points of highest (B) and lowest (D) flow rate, the length of the recirculation zone increases by increasing heart rate from case 1 to case 2. In contrast, at the point of peak flow deceleration (C), increasing heart rate leads to a slight decrease in the length of recirculation region. Increasing heart rate at constant flow rate (i.e., from case 1 to case 3), decreases the length of recirculation zone except at the lowest flow rate. At peak acceleration, the flow remains attached to the walls in all three cases studied. At time point D of the 108 bpm runs, the flow profile contains a region of reverse flow even at the entrance of the common carotid artery due to the fully developed Womersley flow boundary condition associated with the sharp deceleration there.

In contrast, no flow separation was seen along the outside wall of the external carotid (results not shown). Curvature of the external carotid artery failed to produce an adverse pressure gradient of sufficient strength to separate the flow from the outside wall of the artery (the common-external adjoining wall). Comparison of the maximum wall shear stress values in that region (at peak systole) reveals an increase in peak  $\tau_w$  levels from 14.9 to 19.5 Pa with the increase in heart rate from case 1 to case 2, but a much smaller increase to 15.2 Pa in case 3. The same comparison during peak systole at the carotid apex reveals an increase from 15.8 Pa at 72 bpm to 24.7 Pa at 108 bpm in case 2, but a slight decrease to 15.3 Pa in case 3. All of these changes correspond most closely to changes in mean flow rate with the frequency exerting a secondary influence.

Although not explicitly computed, it is possible to infer approximate values for the spatial gradient in  $\tau_w$  from the band plots of Fig. 4 and the instantaneous distributions of Fig. 5. Because there are no significant differences in the overall pattern of  $\tau_w$ , the spatial gradients would follow the same overall tendencies discussed above for  $\tau_w$ .

#### *OSI and Wall Shear Stress Maximum Temporal Gradient*

Two other parameters that have been investigated are the oscillatory shear index (Fig. 6) as defined above<sup>18</sup> and the maximum wall shear stress temporal gradient  $(\partial\tau_w/\partial t)_{\max}$  over the cycle (Fig. 7). Nonzero values of the OSI in all three cases studied are confined to the region of the carotid bulb, with magnitudes and distribution patterns that are notable for their similarity.

The magnitudes of  $(\partial\tau_w/\partial t)_{\max}$  are considerably higher in the 108 bpm case with high flow rate (case 2)

**TABLE 1. Maximum wall shear stress ( $\tau_w$ ) in the carotid bulb and size of the recirculation region at different times during the cardiac cycle: peak acceleration (A), peak flow (B), and peak deceleration (C) as well as at the time of lowest flow rate (D) [see Fig. 3(b)] for the case of a person at rest (72 bpm) and a person exercising moderately (108 bpm). (–) signifies that the wall shear stress vector reversed direction. Length of the recirculation region is defined as the normalized length along the common-internal carotid adjoining wall (line 1 of Fig. 1) with reversed shear stress. The carotid bulb spans the region  $s=0.40-0.73$ , where  $s$  is normalized distance along line 1. Values in parentheses represent the range of  $s$  over which flow reversal occurs.**

Time point in cardiac cycle	72 bpm (case 1)		108 bpm (case 2)		108 bpm (case 3)	
	Max $\tau_w$ in bulb (Pa)	Recirculation length	Max $\tau_w$ in bulb (Pa)	Recirculation length	Max $\tau_w$ in bulb (Pa)	Recirculation length
A	2.0	None	2.5	None	1.8	None
B	2.9	0.09 (0.4 to 0.49)	3.1	0.12 (0.38 to 0.52)	2.	0.06 (0.41 to 0.47)
C	1.8(–)	0.46 (0.32 to 0.78)	1.8(–)	0.44 (0.33 to 0.77)	1.4(–)	0.43 (0.33 to 0.76)
D	0.8(–)	0.45 (0.32 to 0.77)	2.6(–)	0.87 (0 to 0.87)	1.9(–)	0.87 (0 to 0.87)

but contrary to the comparisons of  $\tau_w$ , these differences cannot be explained by the higher flow rates alone. In the common carotid,  $(\partial\tau_w/\partial t)_{\max}$  averages 140 Pa/s (72 bpm) and increases to 215 and 160 Pa/s at 108 bpm, cases 2 and 3, respectively. In the carotid bulb,  $(\partial\tau_w/\partial t)_{\max}$  doubles in value from 35 to 70 and 60 Pa/s with the increase in heart rate at increased flow rate (case 2) and fixed flow rate (case 3), respectively. In contrast,  $(\partial\tau_w/\partial t)_{\max}$  at the region of curvature in the wall adjoining the common-external carotid reaches 285 Pa/s (72 bpm) and 430 and 410 Pa/s at 108 bpm for cases 2 and 3, respectively. At the carotid apex,  $(\partial\tau_w/\partial t)_{\max}$  is an order of magnitude greater than at the bulb and reaches values of 600 Pa/s (72 bpm) and 800 Pa/s at 108 bpm for both cases 2 and 3. Within the external carotid, further down from the region of curvature,  $(\partial\tau_w/\partial t)_{\max}$  is seen to vary between 350 and 500 Pa/s (72 bpm), 550–700 Pa/s (108 bpm) in case 2, and 400–550 Pa/s in case 3.

#### Pressure Drop

Pressure drops were compared at point (C) during the decelerative phase of systole in all cases; this time step experiences some of the largest adverse pressure gradients throughout the cycle (results not shown). A pressure drop (which can be explained largely on the basis of convective rather than temporal acceleration) of 1.0, 1.3, and 0.7 kPa was recorded at this time step in cases 1 to 3, respectively, which is at most only 8% of the applied systolic pressure.

## DISCUSSION

Most of the recent literature on the relationship between hemodynamics and atherosclerosis point to wall shear stress as the most important fluid mechanic parameter. It is now widely accepted<sup>16,18,29</sup> that low  $\tau_w$  regions

are more prone to atherosclerosis. Wall shear stress levels greater than 1.5 Pa are generally believed to induce endothelial quiescence and an atheroprotective gene expression profile, whereas low shear stress levels (less than 1.0 Pa) stimulate an atherogenic phenotype and are generally observed at atherosclerosis-prone sites.<sup>21</sup> This is evident in our  $\tau_w$  results (Figs. 4 and 5). With the increase in heart rate, our results differ, depending on whether or not we allow flow rate to increase. Although, the current study only examines the carotid bifurcation, the two cases at elevated heart rate could be viewed as representing two physiologic limits, the first corresponding to arteries in regions that experience an increase in flow with exercise, and the second corresponding to the regions that do not. In the former case,  $\tau_w$  values are generally higher, nearly 50% higher in some locations, but only in proportion to the increase in flow rate elsewhere, and the low  $\tau_w$  region in the carotid bulb reduces in size. This observation may provide some support to the hypothesis that exercise promotes an atheroprotective phenotype.<sup>12,13</sup>

Our results for case 3, however, when flow rate is held constant, suggest a very different conclusion. Shear stress magnitudes and distribution are virtually unchanged, and are even slightly higher in the carotid bulb at the lower heart rate, at least at times A and C. The similarity between these two cases is strong and somewhat counterintuitive. Because of the high Womersley value at higher heart rates, one would expect to see thinner boundary layers and, consequently, higher peak shear stress values. Even these small differences disappear, however, if we only consider  $(\tau_w)_{\text{ave}}$ , which is as expected because OSI maps (Fig. 6) show very little sign of significant negative shear stress, and hence, Womersley number should have no effect on mean wall shear stress  $(\tau_w)_{\text{ave}}$  if the mean flow is unchanged. [It must be noted that mean wall shear stress  $(\tau_w)_{\text{ave}}$  is calculated

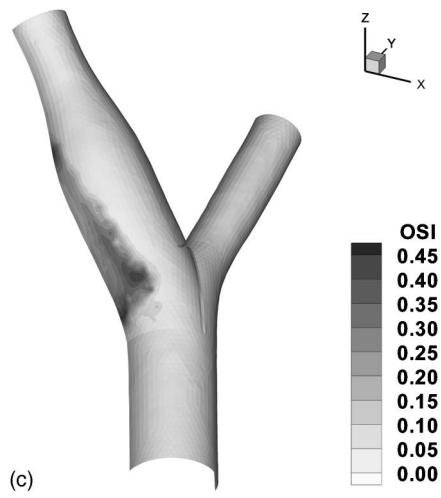
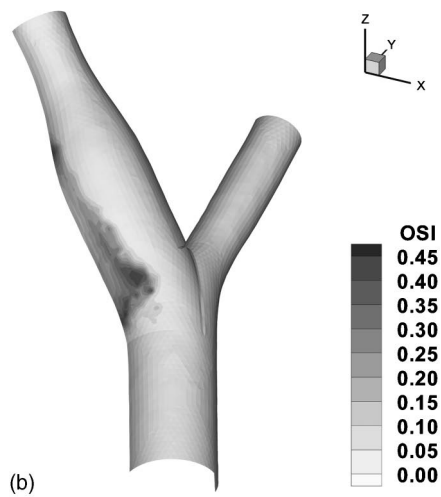
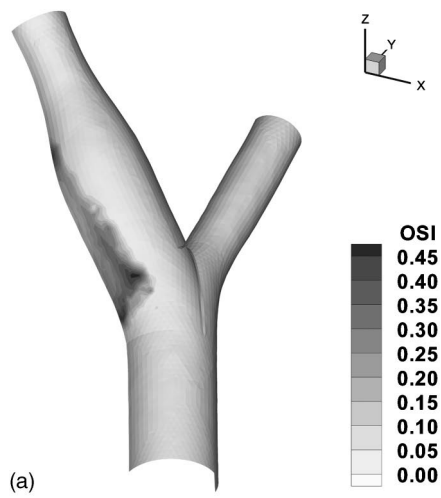


FIGURE 6. Oscillatory shear index (OSI) plots: 72 bpm (a); 108 bpm [(b) and (c)].

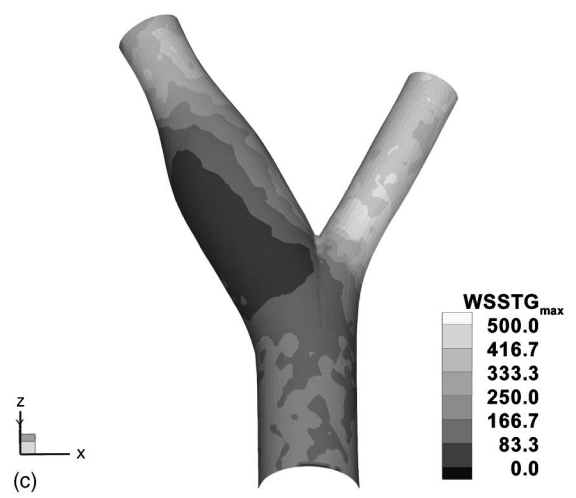
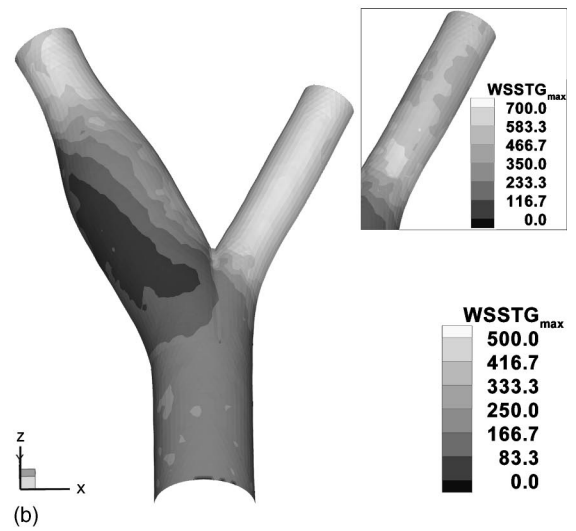
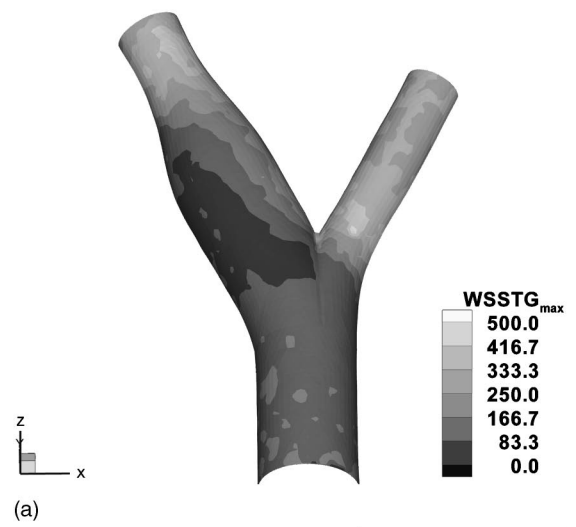


FIGURE 7. Maximum wall shear stress temporal gradient ( $WSSTG_{max} = (\partial\tau_w/\partial t)_{max}$ ) (in Pa/s): 72 bpm (a); 108 bpm [(b) and (c)].

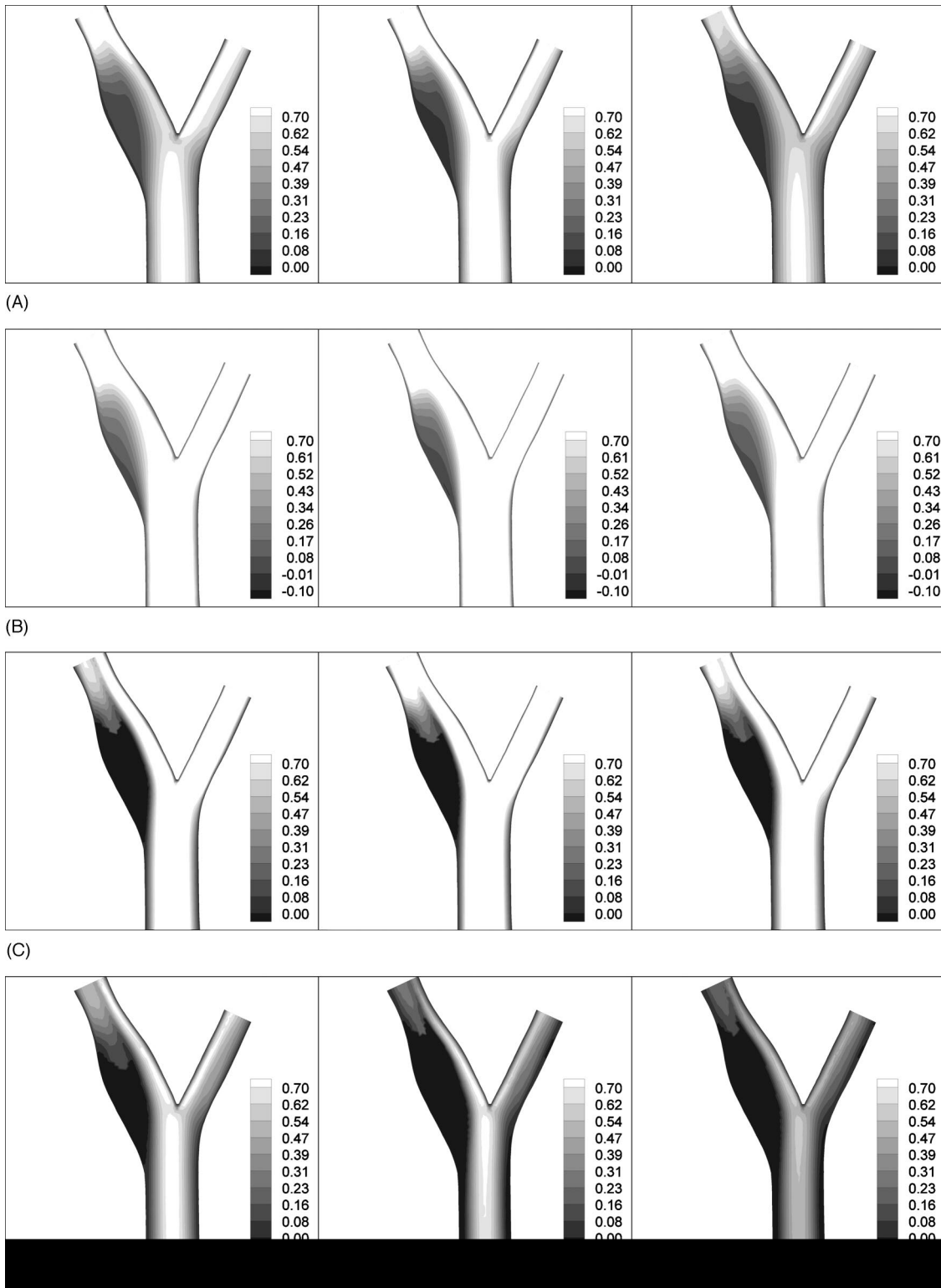


FIGURE 8. Contour plots of velocity magnitude (in m/s) at four time points in the heart cycle. Letters A–D refer to the time points indicated in Fig. 3. Left panel: 72 bpm (case 1); middle panel: 108 bpm (case 2); and right panel: 108 bpm (case 3).

using the *absolute value* of the instantaneous shear stress.]

To further address the little variation in peak wall shear stress as the Womersley number changes, contour plots of velocity magnitude are shown in Fig. 8. As the figures demonstrate, the flow features are qualitatively similar at the time points of interest. The most pronounced difference quantitatively is found at time D, i.e., the point of lowest flow rate, where case 3 shows the considerably slower velocities. Interestingly, cases 1 and 3 are quite similar at time points A–C, despite the different waveform and different Womersley number.

This can be explained by the importance of momentum convective mixing and the resulting tendency of the flow to behave in a nearly quasi-steady manner despite values of the Womersley number in the range of 5.5–7.5 based on the fundamental heart frequency. The mixing, due to secondary flows, essentially increases the effective diffusivity for momentum, and thereby reduces the effective Womersley number. This is supported by the fact that the only pronounced differences in velocity magnitude are experienced at time point D, i.e., where the convective mixing is less dominant. This may be also attributed to the limited effect of Womersley number between values of 5.5 and 7.5 based on the fundamental heart frequency. That is, considering that the Stokes layer is inversely proportional to Womersley number, a change of Womersley number from 5.5 to 7.5 would roughly mean a 25% reduction in the Stokes layer in the unseparated regions. At these Womersley numbers, this reduction does not exert appreciable changes in the velocity magnitude pattern between cases 1 and 3, particularly at higher instantaneous flow rates, i.e., in systole (see Fig. 8, panels A–C as compared to panel D).

This explains the indistinguishable mean wall shear patterns between cases 1 and 3 (see Fig. 4). Of the two high heart rate cases considered (cases 2 and 3), the latter case is probably more relevant. It is believed that during exercise the peripheral resistance in the brain remains fairly constant and instead higher flow rates target the oxygen needing muscles.<sup>5</sup>

The maximum wall shear stress temporal gradient,  $(\partial\tau_w/\partial t)_{\max}$ , has been related to the expression of atherogenesis-related genes in endothelial cells (ECs). Bao *et al.*<sup>1</sup> have found that the temporal gradient in shear but not steady shear stimulates the expression of monocyte chemoattractant protein-1 (MCP-1), a potent chemotactic agent for monocytes, and platelet-derived growth factor A (PDGF-A), a potent mitogen and chemotactic agent for smooth muscle cells. The higher values of  $(\partial\tau_w/\partial t)_{\max}$  experienced during the 108 bpm simulation suggest, therefore, that exercise may lead to another pathway that works to *increase* rather than decrease the atherogenicity of ECs. This, of course, must be considered in the context of the hypothesis that hemodynamic

forces generated by complex flow patterns can act as both positive and negative stimuli in atherogenesis via effects on endothelial cell gene expression.<sup>12</sup> It is well known that endothelial cells in different regions of the arterial tree acquire both functional and dysfunctional phenotypes due to regional hemodynamics.<sup>13</sup> This complex character of endothelial cells may contribute to the notion that atherosclerosis is a multifactorial phenomena. Finally, it must be remarked that the flows in the external carotid are overestimated due to the lack of a tributary there, leading to high temporal gradients of wall shear stress on the external carotid artery during exercise [see Figs. 7(b) and 7(c)].

Recent studies<sup>32,33</sup> suggest that spatial shear stress gradients may play a key role in the morphological remodeling of the vascular endothelium. Tardy *et al.*<sup>32</sup> observed that endothelial cell division increased in the vicinity of flow separation whereas cell loss was elevated both upstream and downstream in the regions where the shear gradient diminished. The current study suggests that exercise results in no significant impact on the overall patterns of  $\tau_w$  and hence the spatial gradients thereof in the carotid bulb, believed to be the early site atherosclerosis.

These solutions also provide insight into the importance of performing a coupled fluid and structure interaction (FSI) solution. Since many codes lack this capability, it is important to assess the need for this additional complexity. The maximum pressure drop along the carotid bifurcation (due to inertial effects) is  $\sim 8\%$  of the systolic pressure. This small change in the wall pressure distribution supports the notion that FSI analyses may not be necessary in assessing the wall mechanical strains when examining arteries with nonsevere stenoses. With respect to the fluid mechanical parameters, Perktold and Rappitsch<sup>27</sup> show that the significant differences in wall shear stress, of up to 25%, only appeared at the divider wall between the distensible and nondistensible models. They observed no difference in wall shear stress between the two models at the primary region of atherogenic interest, the carotid bulb. Thus, in numerical studies aimed at understanding atherogenesis in the carotid bulb, FSI analyses may not be necessary. They may be necessary, however, in cases of severe disease (90% stenoses and above) because blood pressure will be higher, and so will the pressure drop across the stenosis, resulting in larger scale wall motion, even with the presence of a stiffer diseased arterial wall.<sup>3</sup>

We believe the present model is a fair representation of the common characteristics observed in a normal healthy carotid bifurcation. It incorporates a fairly realistic, though idealized, 3D geometry that replicates main geometrical features in typical healthy carotid bifurcations. Further, the arterial wall mechanics involves a nonlinear model using Lagrangian formulation for large

displacements and large strains. It incorporates a strain energy density function that portrays the well known strain-stiffening behavior of healthy arterial wall. Further, the FSI formulation implemented in the present model takes into account the artery wall compliance, which can have locally significant hemodynamics effects. Therefore, the model has the essential features that govern the carotid bifurcation hemodynamics in normal healthy human subjects. To investigate the impact of detailed anatomical and morphological features that are specific to different human subjects would, however, require subject-specific models based on *in vivo* images of the carotid bifurcation.

Finally, it is important to note that exercise affects the cardiovascular system via a complex mechanism, giving rise to a wide range of changes in the dynamics of the system. Here, we only focused on the carotid bifurcation and studied how a relatively narrow range of physiologically conceivable changes in carotid artery blood flow would impact the atherogenically relevant hemodynamic patterns experienced therein. A detailed analysis of the effect of exercise requires a comprehensive model of the whole cardiovascular network, incorporating various dynamical and neural pathways that play a role in this complex mechanism.<sup>20</sup>

### ACKNOWLEDGMENTS

Support from the National Heart, Lung, and Blood Institute (Grant No. HL61794) is gratefully acknowledged. The authors gratefully acknowledge fruitful discussions with Thomas Heldt. The first two authors (H.F.Y. and M.R.K.) equally contributed to this work.

### REFERENCES

- <sup>1</sup>Bao, X., C. Lu, and J. A. Frangos. Temporal gradient in shear but not steady shear stress induces PDGF-A and MCP-1 expression in endothelial cells: Role of NO, NF kappa B, and egr-1. *Arterioscler. Thromb., Vasc. Biol.* 19:996–1003, 1999.
- <sup>2</sup>Bathe, K. J. *Finite Element Procedures*. Englewood Cliffs, NJ: Prentice-Hall, 1996.
- <sup>3</sup>Bathe, M., and R. D. Kamm. Fluid–structure interaction finite element analysis of pulsatile blood flow through a compliant stenotic artery. *J. Biomech. Eng.* 121:361–369, 1999.
- <sup>4</sup>Berger, S. A., and L. D. Jou. Flows in stenotic vessels. *Annu. Rev. Fluid Mech.* 32:347–384, 2000.
- <sup>5</sup>Berne, R. M., and M. N. Levy. *Cardiovascular Physiology*, 7th ed. Toronto: Mosby, 1997.
- <sup>6</sup>Bharadvaj, B. K., R. F. Mabon, and D. P. Giddens. Steady flow in a model of the human carotid bifurcation. Part I—Flow visualization. *J. Biomech.* 15:349–362, 1982.
- <sup>7</sup>Bharadvaj, B. K., R. F. Mabon, and D. P. Giddens. Steady flow in a model of the human carotid bifurcation. Part II—Laser–Doppler anemometer measurements. *J. Biomech.* 15:363–378, 1982.
- <sup>8</sup>Delfino, A. Analysis of stress field in a model of the human carotid bifurcation. In: Department of Physics. Ecole Polytechnique Federale de Lausanne: Lausanne, Switzerland, 1996.
- <sup>9</sup>Delfino, A., N. Stergiopoulos, J. E. Moore, Jr., and J. J. Meister. Residual strain effects on the stress field in a thick wall finite element model of the human carotid bifurcation. *J. Biomech.* 30:777–786, 1997.
- <sup>10</sup>Downing, J. M., and D. N. Ku. Effects of frictional losses and pulsatile flow on the collapse of stenotic arteries. *J. Biomech. Eng.* 119:317–324, 1997.
- <sup>11</sup>Friedman, M. H., C. B. Barger, D. D. Duncan, G. M. Hutchins, and F. F. Mark. Effects of arterial compliance and non-Newtonian rheology on correlations between intimal thickness and wall shear. *J. Biomech. Eng.* 114:317–320, 1992.
- <sup>12</sup>Garcia-Cardena, G., J. Comander, K. R. Anderson, B. R. Blackman, and M. A. Gimbrone, Jr. Biomechanical activation of vascular endothelium as a determinant of its functional phenotype. *Proc. Natl. Acad. Sci. U.S.A.* 98:4478–4485, 2001.
- <sup>13</sup>Garcia-Cardena, G., J. I. Comander, B. R. Blackman, K. R. Anderson, and M. A. Gimbrone. Mechanosensitive endothelial gene expression profiles: Scripts for the role of hemodynamics in atherogenesis? *Ann. N.Y. Acad. Sci.* 947:1–6, 2001.
- <sup>14</sup>Gijsen, F. J., F. N. van de Vosse, and J. D. Janssen. The influence of the non-Newtonian properties of blood on the flow in large arteries: Steady flow in a carotid bifurcation model. *J. Biomech.* 32:601–608, 1999.
- <sup>15</sup>He, X., D. N. Ku, and J. E. Moore, Jr. Simple calculation of the velocity profiles for pulsatile flow in a blood vessel using Mathematica. *Ann. Biomed. Eng.* 21:45–49, 1993.
- <sup>16</sup>Ku, D. N. Blood flow in arteries. *Annu. Rev. Fluid Mech.* 32:346–384, 1997.
- <sup>17</sup>Ku, D. N., and D. P. Giddens. Laser Doppler anemometer measurements of pulsatile flow in a model carotid bifurcation. *J. Biomech.* 20:407–421, 1987.
- <sup>18</sup>Ku, D. N., D. P. Giddens, C. K. Zarins, and S. Glagov. Pulsatile flow and atherosclerosis in the human carotid bifurcation. Positive correlation between plaque location and low oscillating shear stress. *Arteriosclerosis (Dallas)* 5:293–302, 1985.
- <sup>19</sup>Kuban, B. D., and M. H. Friedman. The effect of pulsatile frequency on wall shear in a compliant cast of a human aortic bifurcation. *J. Biomech. Eng.* 117:219–223, 1995.
- <sup>20</sup>Magosso, E., S. Cavalcanti, and M. Ursino. Theoretical analysis of rest and exercise hemodynamics in patients with total cavopulmonary connection. *Am. J. Physiol. Heart Circ. Physiol.* 282:H1018–1034, 2002.
- <sup>21</sup>Malek, A. M., S. L. Alper, and S. Izumo. Hemodynamic shear stress and its role in atherosclerosis. *J. Am. Med. Assoc.* 282:2035–2042, 1999.
- <sup>22</sup>Moore, Jr., J. E., N. Guggenheim, A. Delfino, P. A. Doriot, P. A. Dorsaz, W. Rutishauser, and J. J. Meister. Preliminary analysis of the effects of blood vessel movement on blood flow patterns in the coronary arteries. *J. Biomech. Eng.* 116:302–306, 1994.
- <sup>23</sup>Moore, Jr., J. E., and D. N. Ku. Pulsatile velocity measurements in a model of the human abdominal aorta under resting conditions. *J. Biomech. Eng.* 116:337–346, 1994.
- <sup>24</sup>Moore, Jr., J. E., D. N. Ku, C. K. Zarins, and S. Glagov. Pulsatile flow visualization in the abdominal aorta under differing physiologic conditions: Implications for increased sus-

- ceptibility to atherosclerosis. *J. Biomech. Eng.* 114:391–397, 1992.
- <sup>25</sup>Moore, Jr., J. E., C. Xu, S. Glagov, C. K. Zarins, and D. N. Ku. Fluid wall shear stress measurements in a model of the human abdominal aorta: Oscillatory behavior and relationship to atherosclerosis. *Atherosclerosis* 110:225–240, 1994.
- <sup>26</sup>Ozawa, E. T., Bottom, K. E., Xiao, X., and Kamm, R. D. Numerical simulation of enhanced external counterpulsation. *Ann. Biomed. Eng.* 29:284–297, 2001.
- <sup>27</sup>Perktold, K., and G. Rappitsch. Computer simulation of local blood flow and vessel mechanics in a compliant carotid artery bifurcation model. *J. Biomech.* 28:845–856, 1995.
- <sup>28</sup>Perktold, K., M. Resch, and H. Florian. Pulsatile non-Newtonian flow characteristics in a three-dimensional human carotid bifurcation model. *J. Biomech. Eng.* 113:464–475, 1991.
- <sup>29</sup>Ross, R. Atherosclerosis—An inflammatory disease. *N. Engl. J. Med.* 340:115–126, 1999.
- <sup>30</sup>Steinman, D. A., and C. R. Ethier. The effect of wall distensibility on flow in a two-dimensional end-to-side anastomosis. *J. Biomech. Eng.* 116:294–301, 1994.
- <sup>31</sup>Tang, D., Yang, J., Yang, C., and Ku, D. N. A nonlinear axisymmetric model with fluid–wall interactions for steady viscous flow in stenotic elastic tubes. *J. Biomech. Eng.* 121:494–501, 1999.
- <sup>32</sup>Tardy, Y., N. Resnick, T. Nagel, M. A. Gimbrone, and C. F. Dewey, Jr. Shear stress gradients remodel endothelial monolayers *in vitro* via a cell proliferation–migration–loss cycle. *Arterioscler., Thromb., Vasc. Biol.* 17:3102–3106, 1997.
- <sup>33</sup>Topper, J. N., and M. A. Gimbrone, Jr. Blood flow and vascular gene expression: Fluid shear stress as a modulator of endothelial phenotype. *Mol. Med. Today* 5:40–46, 1999.
- <sup>34</sup>Younis, H. F., C. I. Chung, and R. D. Kamm. Challenges in developing an accurate model for carotid bifurcation blood flow and wall mechanics. In: *Computational Fluid and Solid Mechanics*, edited by K. J. Bathe., Vol. 2, pp. 1434–1439, 2001.
- <sup>35</sup>Zhao, S. Z., X. Y. Xu, A. D. Hughes, S. A. Thom, A. V. Stanton, B. Ariff, and Q. Long. Blood flow and vessel mechanics in a physiologically realistic model of a human carotid arterial bifurcation. *J. Biomech.* 33:975–984, 2000.